R. Benvenuto, M. Lavagna, S. Salvi
Multibody Dynamics Driving GNC and System Design in Tethered Nets for Active Debris Removal
Advances in Space Research, Vol. 58, N. 1, 2016, p. 45-63
doi:10.1016/j.asr.2016.04.015

Multibody dynamics driving GNC and system design in tethered nets for active debris removal

Riccardo Benvenuto *, Michèle Lavagna, Samuele Salvi

Department of Aerospace Science and Technologies, Politecnico di Milano, Via La Masa 34, 20156 Milano, Italy

Abstract

Debris removal in Earth orbits is an urgent issue to be faced for space exploitation durability. Among different techniques, tethered-nets present appealing benefits and some open points to fix. Former and latter are discussed in the paper, supported by the exploitation of a multibody dynamics tool. With respect to other proposed capture mechanisms, tethered-net solutions are characterised by a safer capturing distance, a passive angular momentum damping effect and the highest flexibility to unknown shape, material and attitude of the target to interface with. They also allow not considering the centre of gravity alignment with thrust axis as a constraint, as it is for any rigid link solution. Furthermore, the introduction of a closing thread around the net perimeter ensures safer and more reliable grasping and holding.

In the paper, a six degrees of freedom multibody dynamics simulator is presented: it was developed at Politecnico di Milano – Department of Aerospace Science and Technologies – and it is able to describe the orbital and attitude dynamics of tethered-nets systems and end-bodies during different phases, with great flexibility in dealing with different topologies and configurations. Critical phases as impact and wrapping are analysed by simulation to address the tethered-stack controllability. It is shown how the role of contact modelling is fundamental to describe the coupled dynamics: it is demonstrated, as a major novel contribution, how friction between the net and a tumbling target allows reducing its angular motion, stabilizing the system and allowing safer towing operations. Moreover, the so-called tethered space tug is analysed: after capture, the two objects, one passive and one active, are connected by the tethered-net flexible link, the motion of the system being excited by the active spacecraft thrusters. The critical modes prevention during this phase, by means of a closed-loop control synthesis is shown. Finally, the connection between flexible dynamics and capture system design is highlighted, giving engineering answers to most challenging open points to lead to a ready to flight solution.

Keywords: Active debris removal; Tethered-net systems; Multibody dynamics; Contact dynamics; GNC design

1. Introduction

The steadily increase of the space debris population around Earth is threatening the future of space utilisation for both commercial and scientific purposes: therefore, both a disposal policy to properly manage new space vehicles end-of-life, and active debris removal (ADR) are necessary to guarantee safe operational life time for space systems in Earth orbit. In particular, the ADR falls in the remediation area, focused on trading-off, designing and implementing dedicated missions to remove inactive satellites and dangerous existing debris from space; the most relevant challenge for those class of missions is represented by the debris capture solution implementation, to be brought by an active platform, nearby the target, chasing, capturing and removing it reliably, whatever the shape and

* Corresponding author.
E-mail addresses: riccardo.benvenuto@polimi.it (R. Benvenuto),

the dynamics of the target is. Recent studies run by NASA (Liou and Johnson, 2007) and ESA (Bastida and Krag, 2011) revealed that the environment can be stabilized if objects in the order of 5 to 10 per year are removed from space; more, the priority debris list follows the more massive in highly inclined orbits the more urgent rule being, in such a case, ADR more effective in collisions occurrence and dangerous cascade effects reduction. As far as the capture and removal strategy is looked at, it is straightforward that the more the general purpose it is the more cost effective would be, but on the other side, the less effective it may turn to be. In fact, a general-purpose removal system should effectively intervene on objects different in configuration, materials and possibly in dimensions. Moreover, target to be captured do not cooperate and have a complex, free, not completely a priori known dynamics.

Different techniques were proposed for ADR and servicing, starting from more conventional rigid docking mechanisms, to tentacles, harpoons and throwing-nets, up to techniques with no contact at all, as the ion beam shepherd, proposed by Bombardelli and Pelaez (2011) and exploiting gas plume momentum exchange or drag augmentation devices, as expanding foams proposed by Andrenucci et al. (2011), both in the framework of ESA's Ariadna studies. Rigid docking devices and robotic arms were proposed by Hobbs (2010) and Reed et al. (2012) and derive their concepts from various mechanisms that have been developed over the past 20 years (Gonzalez-Vallajo et al., 1992; Hardt et al., 2011). Many studies were carried out on the arm dynamics and its interaction with the non-cooperative vehicle, for example by Seweryn et al. (2011) at ESA or in the framework of DEOS – Deutsche Orbitale Servicing Mission by Astrium and DLR (Rank et al., 2011). However, clamping mechanisms are all basically dependent on the shape of the target and require fine relative attitude and position control, face to an uncontrolled and partially unknown object.

As mentioned above, flexible techniques have recently been studied: they are characterised by establishing a tethered connection between the two bodies and they all present similar characteristics related to the post-capture manoeuvring and control (and therefore similar advantages and drawbacks), although differentiating for the capturing device itself and the grabbing operations. The obtained tethered system is the so-called tethered space tug: after capture, the two objects, one passive and one active, are connected by the tethered-net flexible link, the motion of the system being excited by the active spacecraft thrusters. The tethered tug was firstly studied by Aslanov and Yudintsev (2013a, 2013b), Jasper et al. (2012), and Jasper and Schaub (2013) who independently studied different control techniques using a simplified simulation environment. On the other hand, as far as the capture device is concerned, a Harpoon prototype was built at Astrium (Reed et al., 2012) and tested repeatedly against representative satellite material. Nishida and Yoshikawa (2003, 2007), proposed flexible tentacles to grab the debris objects and damp its residual motion through the mechanism flexibility. Huang et al. (2015a, 2015b) and Wang et al. (2015) studied with great detail the Tethered-Space-Robot dynamics and control: it consists of a small controlled vehicle tethered-connected to the chaser, responsible to grab the target and establish the connection. This technique presents the advantage of being less intrusive (i.e. safer) and more reliable with respect to the harpoon; it also guarantees a safer distance from the tumbling target with respect to the tentacles solution.

The use of throw-nets and tow-tethers has also been advocated as one of the preferred solutions: a flexible capture net is cast from an active satellite by impulsively accelerating a number of flying weights, hereinafter named bullets, attached to the net mouth; then the relative trajectory of the bullets deploys the capture net gradually during the flying process; finally the net wraps the debris element, closes around it and thanks to the active chaser, tethered connected with the net, drag it to the disposal location in space. The concept of tethered-net satellite capture is represented in Fig. 1. The greatest advantages of tethered-net systems with respect to other proposed capture mechanisms are traceable in the higher interfaceability towards unknown targets' physical and dynamics characteristics, isotropic loads and safer (i.e. larger) capturing distances. The capture distance depends on the net configuration and size: the distance is tuned so that the net impacts with the target when it is completely deployed. Furthermore, in contrast with rigid capture systems (as robotic arms), these capture techniques do not need fine relative attitude control (the net can be shot almost independently of target relative attitude and tumbling, relying on the impact and entanglement for capture and on the friction for relative motion/tumbling dissipation). They also allow not to considering the centre of gravity alignment with thrust axis as a constraint, as it is for any rigid link solution: pulling the target instead of pushing it, as in the case of rigid connections, makes the system once again independent of target attitude, because the pulling force distributes along the

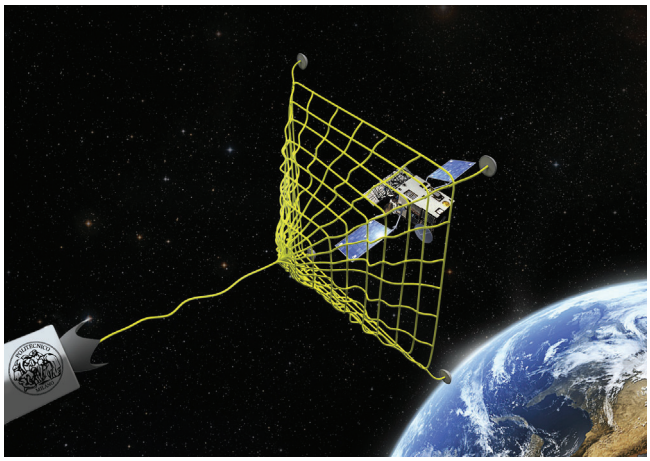

Fig. 1. Tethered-net capture concept.

tether and is always inline with the target centre of mass. On the contrary, in the case of rigid links, the pushing force needs to be controlled, not to impose torques on the whole stack, leading to an increase complexity in the attitude control, being normally the debris centre of mass unknown. On the other hand, these techniques are characterised by the difficulty in robustly detect the capture and closure occurrence after the impact and by settling a flexible tethered connection between the chaser and the target. The latter opens new challenges for guidance navigation and control (GNC) design: the chaser GNC system is required to be precise enough to gain stabilized specific relative orbits and to robustly perform de/re-orbiting operations, while controlling a complex system and damping vibrations of flexible elements and connections.

Nowadays the European community, working on large space debris active removal methodologies, accomplished feasibility and phase A studies focused on setting the system requirements and addressing the most promising technologies to be further investigated up to the final implementation (Wormnes et al., 2013a), identifying the net as one of the candidate solutions. The system was firstly studied by Astrium from a systemic point of view: in the ROGER study (2003), a system for re-orbiting GEO satellites was designed, where a net with four weights was deployed by the use of spring mechanisms in order to capture the non-cooperative target satellite. Different control strategies of the net-tether system were taken into consideration, depending on the rotation state of the target. More recently, the e.Deorbit study (Biesbroek et al., 2013) was conducted by ESA's Concurrent Design Facility (CDF) within the Clean Space Initiative on a system design for the most promising ADR options. The net-tether option was selected as one of the suitable candidates and a preliminary system design was carried out. Within the e.Deorbit study, multibody simulations of around 6000 DOF per simulation (Wormnes, 2013b) were performed using a physic engine derived from game development environment (cf. Blender), and analyzing the sensitivity with respect to parameters as tether physical characteristics (length, stiffness, material damping), controllers, relative velocity and rotation rates. Botta et al. (2015) also studied the net dynamics, focusing on the contact dynamics and analysing different non-linear model for damping term computation in the Hunt–Crossley model (cf. Section 2.2). However, the friction and the reactions on end-bodies were not yet introduced. Recently, Huang et al. (2015c), introduced the Manoeuvring-Net Space Robot System, where bullets or flying masses are substituted by small controlled vehicles able to actively control the net trajectory and deployment, increasing the reliability of this system with respect to the purely passive ones.

The work described in this paper aims at taking the technology a step forward by developing a validated full six degrees of freedom multibody simulator, useful for GNC and system design, including contact dynamics and reactions on vehicles. The problem has been deeply analysed to simulate at the best the net deployment, contact and closure dynamics on the target. A dedicated numerical tool has been developed at Politecnico di Milano – Department of Aerospace Science and Technologies (PoliMi-DAER), to simulate the entire stack dynamics, in order to support the overall system design, to synthetize more reliable and adapted GNC laws and to ensure the mission reliability for such a delicate task. The software has been verified and validated through benchmarking with analytical and on ground experimental results to be further confirmed by the parabolic flight test campaign performed in June 2015, whose data are currently being analysed. This paper firstly provides a description of the mathematical models the tool is based on: the multibody constrained dynamics have been represented through a discretized viscoelastic model for the flexible components, and taking into account the six degrees of freedom end-satellites. The system dynamics is investigated in non-uniform Earth gravity field, under aerodynamic drag, solar pressure and control forces, whenever applicable.

A hierarchical collision detection algorithm and a refined contact law that also accounts for friction between the net and the target are also implemented in the model and discussed in the paper, focusing in particular on the fallouts of contact modelling on the stack behaviour and controllability. Tumbling target capture and towing scenarios simulations are discussed: in a model not accounting for friction between different elements, the evolution of target angular velocity shows the so-called tail wagging effect, i.e. the periodic oscillation of the debris which appears as a stable limit cycle obtained after a short transient during towing. On the other hand, the complete refined net model allows to appreciate the higher fidelity to the physics of the phenomenon: the introduction of friction, causing energy dissipation thanks to the relative motion of the target debris inside the net, allows demonstrating that the energy dissipation through contact and slippage is responsible for reducing the tumbling target angular momentum, passively damping its angular motion. This effect is extremely important from a control point of view, helping the stabilization of the stack: it is demonstrated how the passive angular motion damping allows the chaser to keep the control authority during the most delicate phases of the mission.

The possibility of critical modes of the system motion leading to destabilization and entanglement of the tether is also discussed, supported by the simulations results: it is demonstrated how closed-loop control laws significantly reduce the likelihood of whiplash effects and post-burn collisions. The control robustness is proved against system uncertainties, especially concerning target features, and external perturbations, as air drag, playing a fundamental role during re-entry.

Eventually, the capture system design is addressed and the design drivers are formulated as an outcome of the dynamics analysis results and the reliability and safety must: influences of the system key parameters, i.e. elasticity and damping, on the dynamics and controllability are

discussed. The tether and net material and shaping are the key feature of such a system: they must be appropriately light, strong and elastic. In particular, their elasticity strongly influences the overall dynamics behaviour: the trade-off of different candidate materials and ropes is presented. To fully characterise the fibre ropes' mechanical properties, including damping, tensile tests and dynamical-mechanical tests have been conducted at PoliMi-DAER laboratories. A critical discussion is added about the effectiveness of a planar net versus a 3D (either conical or pyramidal shape) net configuration solution according to the size, mass and configuration of the class of targets to be wrapped; a net configuration design, allowing reducing the system mass, is also proposed. The paper eventually discusses the design of the net mouth closing mechanism after impact and wrapping around the target. The closure of the net around the target can in fact occur through free entanglement or through a controlled embedded closing device designed and installed directly on the net frontal opening edge, where winches are placed to retrieve closing strings when commanded, as shown in following simulation examples. A closing device would assure a firmer grasping than the closure relying on wrapping and entanglement, avoiding slippage and limiting the risk of failure during the thrusting phase.

2. Multibody dynamics simulation environment

In this section, the multibody dynamics simulation environment is presented. The tool has been developed in house at PoliMi-DAER, to reliably model the dynamics of tethered-net ADR systems and effectively serve as a tool to support system design and to allow control laws implementation, testing and validation.

To guarantee good performances in terms of computational time, lumped parameters methods have been chosen. These models also allow:

- to describe net large deformations and to only include positive tension on the tethers, due to the inability of net's material to withstand compression;
- to tune the accuracy by modifying the number of discretizing elements;
- to parametrically treat different materials and exploit ad-hoc viscoelastic laws;
- to treat general net topologies and configurations, both folded and deployed;
- to obtain a system of explicit ordinary differential equations (ODE).

The chaser and the target are modelled as six degrees of freedom bodies, as well as the bullets, through Newton's and Euler's laws for translational and rotational dynamics. All reactions on bodies due to tethered-net system are taken into account. The system dynamics are subject to the full range of forces and torques expected in Earth orbit. Dealing with these systems, it is important to precisely model the environmental effects: in particular, the gravity and its gradient are important when dealing with long tethers. The atmospheric density also plays an important role both for its increasing magnitude during de-orbit and for its gradient along long tethers or large nets. The spatial motion of the system is studied in non-uniform Earth gravity field, under the action of chaser de-orbiting thrusters (when applicable), aerodynamic drag and solar pressure, which are taken into account as external perturbations on all the elements composing the system, both flexible and rigid.

The simulator has been implemented in Matlab/Simulink, and the obtained large system of ODE is solved by exploiting the software's built-in integration capabilities, with Runge–Kutta methods, after auto-coding it in C++ to improve time performances.

2.1. Flexible dynamics model

The simplest and yet most efficient way to describe a flexible body, that does not withstand compression, is to model it as series of point masses connected by springs-dashpots: the constitutive law of the material can be modelled through the combination of spring-dampers resulting in different tension laws. In Fig. 2, the discretization of a

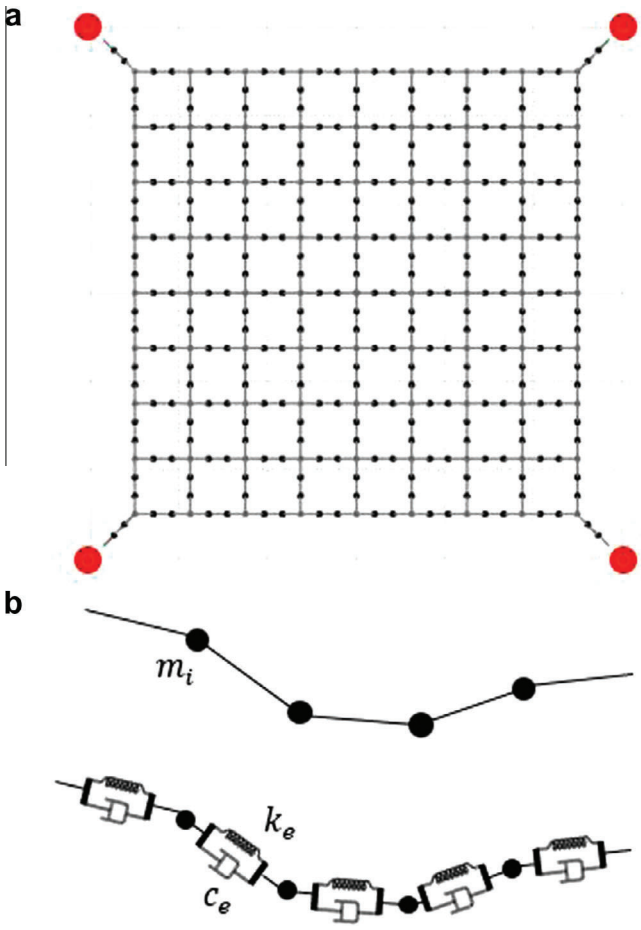

Fig. 2. Tethered-net model and discretization.

planar net is depicted along with a representation of the tether physical model, each net's thread being modelled as a tether.

The linear Kelvin–Voigt model has been chosen here because of the direct relationship of its coefficient with material mechanical properties. Tension on rope elements can be expressed as in Eq. (1) below:

$$T_{i,j} = \begin{cases} [-k_{ij}(|R_{ij}| - l_{nom}) - d_{ij}(V_{ij} \cdot \hat{R}_{ij})]\hat{R}_{ij} & if\,|R_{ij}| > l_{nom} \\ 0 & if\,|R_{ij}| \leqslant l_{nom} \end{cases} \tag{1}$$

where k_{ij} and d_{ij} are the elastic and viscous parameters of element ij (i.e. between node i and j), l_{nom} is the nominal un-stretched length of the tether element, R_{ij} and V_{ij} are, respectively, the relative position and velocity between two consecutive masses (the hat indicating the normalised vector). The stiffness is directly related to material and rope properties, being the axial stiffness defined as in Eq. (2) below:

$$k_{ij} = \frac{EA}{l_{nom}} \tag{2}$$

where E is the Young's modulus and A is the tether cross section. The damping is directly related to the tether mass and natural frequency through its damping ratio ξ as in Eq. (3) below:

$$d_{ij} = 2\xi\sqrt{m_{ij}k_{ij}} \tag{3}$$

Damping ratio and Young's modulus have been determined experimentally at PoliMi-DAER premises for different synthetic fibre ropes that are suitable candidate for these particular ADR systems and meet the requirements on strength and stiffness. It is to note that the expression for tension given in Eq. (1), when the extension is small, for certain directions and values of velocity, may results in a negative tension, giving non-physical results. Practically, this never happens due to the fact that the damping coefficients is several orders of magnitude smaller than the stiffness term; however, a further check has been included in the algorithm for physical consistency, that annuls the tension whenever it becomes negative.

A clarification is worth about the computation of aerodynamics forces on the tether. To ease their computation every half of the tether part connecting two point masses has been assumed as rigid, therefore moving at the same speed of the node competing to it (this model was firstly presented by Aslanov and Ledkov (2012)), as explained in Fig. 3.

With such hypothesis the force acting on a node can be computed as in Eq. (4):

$$Fa_i = \frac{\rho v_i d}{4} c_d \left(\frac{\mathbf{n}_i}{r_{i,i-1}} + \frac{\mathbf{n}_{i+1}}{r_{i+1,i}} \right) \tag{4}$$

where ρ is the atmosphere density, function of the altitude, v_i the velocity of mass i, d the tether diameter, c_d the drag

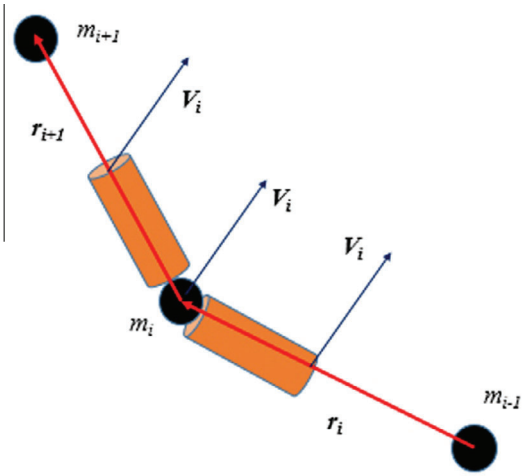

Fig. 3. Tether model for aerodynamics forces computation.

coefficient and $r_{i,i-1}$ the distance between element i and $i-1$. The vector $\boldsymbol{n_i}$ is computed as in Eq. (5):

$$\mathbf{n}_i = (V_i \times r_i) \times r_i \tag{5}$$

2.2. Collision detection and contact dynamics models

Multiple contact events are expected to occur during capture and wrapping phases, both among different parts of the net and between the net and the target. As a result, the representation of the effect of contacts between the bodies is a key to the fidelity of the simulation to reality.

A hierarchical bounding-boxes collision detection algorithm (as detailed in Zachmann (2000)) has been set-up. It consists of an n-phases algorithm refining the zone of contact, in order to select the specific subsystems of discretization nodes to be cross-checked for collision. The control boxes considered are minimum spherical bounding boxes, (MSBB). The selected MSBB method allows a fast and precise treatment of the impact of the net with borders and edges. Furthermore, it well adapts to the discretization of the net/threads in point masses, allowing a simple management of collision detection and contact algorithms.

Many approaches are available to model contact dynamics (as presented in Gilardi and Sharf (2002)). Here a regularized contact models has been adopted: the regularization consists in the reformulation of the problem, changing the nature of the impact from a discontinuous process into a continuous one. The contact forces are described as a function of the contact deformation by smothering the discontinuity of the impact and friction forces in the constraints. This approach is also referred as "penalty method", since the model returns a measure of the constraint violation, the larger the violation, the higher the penalty. In contrast to the contact models based on the rigid body assumption, compliant models describe the rate-dependent normal and tangential compliance relations over time. These models can be easily integrated within the simulation environment based on ODE solvers and

the formulation provides the required degree of freedom necessary to regulate and adjust the contact parameters according to the experimental results.

Furthermore, a point contact model theory is valid as long as the contact region is small, compared to the dimensions of the colliding bodies, and this holds for the aforementioned net modelling. The contact model takes the form of a lumped-parameter spring-damper. The representation scheme and sign convention for both normal and tangential forces is represented in Fig. 4.

Therefore, the local deformation can be parameterized as a function of the penetration depth between the non-deformed bodies. This produces a single algebraic expression relating the inter-penetration to the normal contact force. For direct central frictionless impacts, Hunt and Crossley has proven to be a valid contact model (Hunt and Crossley, 1975), which integrate the Hertz theory (spring model) with a damper in order to take into account the energy dissipation in the impact normal direction. The compliant normal-force expression, proposed by Hunt and Crossley for direct central and frictionless impact, is a non-linear spring-damper model, as in Eq. (6):

$$F_n = -k_c x^n - \lambda x^n \dot{x} \tag{6}$$

where:

- k_c is the equivalent stiffness, Eq. (7) and λ is the hysteresis damping factor;
- n is an empirically coefficient related to the impacting geometries;
- x and $\dot{x}$ are respectively the penetration depth and velocity.

This damped model is consistent with the expectation that the total contact force should vanish whenever the penetration depth goes to zero. This means that no impulsive

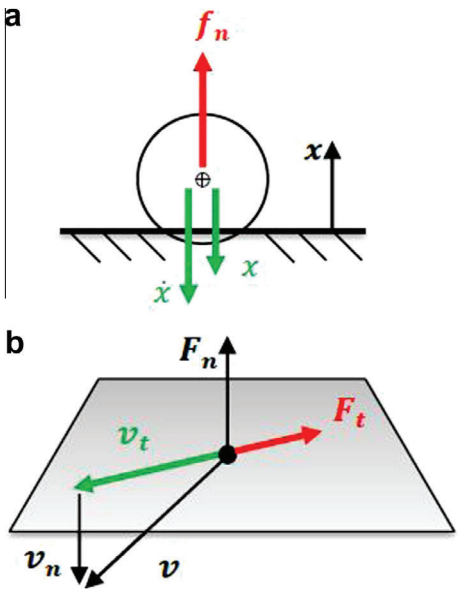

Fig. 4. Representation scheme and convention for normal and tangential contact forces.

behaviour of the contact force dynamics appears at impact. As visible in Fig. 5 on the left, in the case of a linear spring-damper model (such as Kelvin–Voigt, as in Eq. (1)), the contact force is non-null at contact occurrence even with null penetration, negative at the end of the impact phase. This behaviour contradicts two characteristics that are expected from a consistent model:

- contact force equal to zero at zero-penetration;
- contact force always positive, to avoid sticking effect.

Assuming that the energy dissipated (area inside the loop) during the compressive phase (blue) and the one dissipated during the expansion phase (red) are equal, Hunt and Crossley (1975) approximate the hysteresis damping factor as in Eq. (7):

$$\lambda = \frac{3}{2}\alpha k_c \tag{7}$$

where α is an experimental parameter that usually varies in the range [0.08–0.32] s/m and relates the coefficient of restitution e to the impact initial normal velocity as in Eq. (8):

$$e = 1 - \alpha v_n^i \tag{8}$$

Finally, in order to define the contact stiffness coefficients, a few reasonable assumptions were made: first, all contacts are supposed to be elastic; second, the nodes of the net are approximated to spheres consistently with the collision detection algorithm discretization; finally, the debris is expected to be much bigger than each node of the net, therefore the contact between net and debris can be thought as the result of multiple contacts among a sphere and a plane. As a consequence, apart from some special cases (e.g. a node impacting a corner of the debris), impact happens between two continuous and non-conforming surfaces, which make first contact at a point and for which the resulting stresses are highly concentrated. Within these assumptions, Hertzian contact theory is valid and it is possible to use the well-known results (Johnson, 1987) summarized below in Eqs. (9) and (10), where r is the sphere radius. According to Hertzian theory, n appearing in Eq. (6) is equal to 1.5.

$$k_c = \frac{4}{3\pi}\frac{\sqrt{r}}{h_1 + h_2} \tag{9}$$

$$h_i = \frac{1 - v_i^2}{\pi E_i} \tag{10}$$

Contact model implementation has been verified by simulating simpler test cases. Results have proven to be coherent with theory and the physics of the phenomenon, i.e. the contact force is always positive and non-impulsive and the total energy (including the dissipated part) is conserved.

2.3. Friction model

A regularized version of the Coulomb's law of dry friction has been adopted: the proposed semi-empirical model

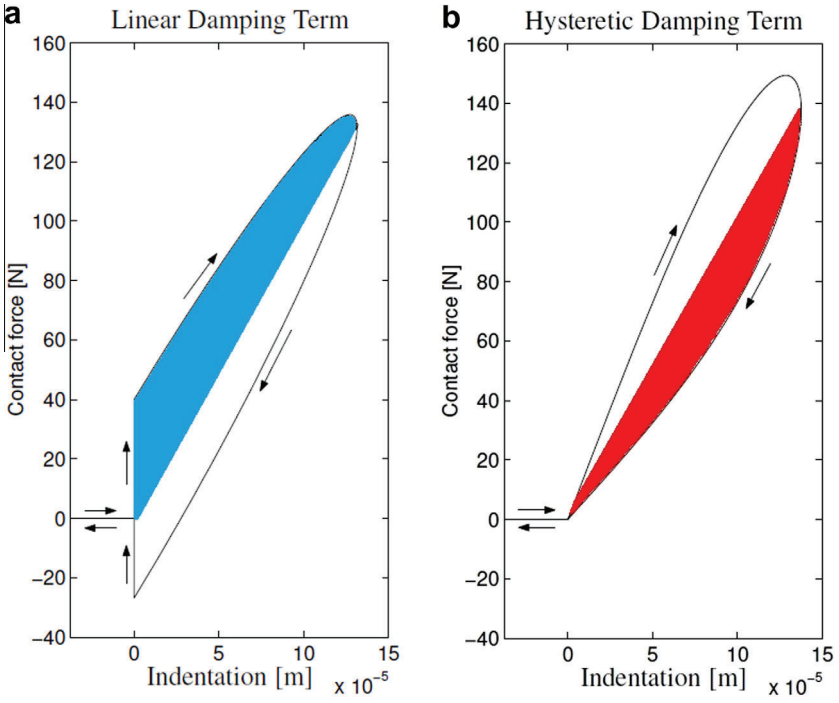

Fig. 5. Linear vs. hysteretic damping in normal contact force model.

is based on the so-called "Dwell Time Dependency" theory of friction, which theorizes a time depending behaviour of stiction forces below a velocity threshold. It is called static friction or stiction, the one occurring below a force threshold proportional to the acting normal contact force F_n, according to the Coulomb's static friction coefficient μ_s as in Eq. (11):

$$F_t \leqslant \mu_s |F_n| \tag{11}$$

Experimental observations have shown that the full magnitude of the stiction force does not come into effect as soon as the relative velocity becomes zero (Rabinowicz, 1956). Instead, the maximum static friction force gradually increases over time and eventually reaches its upper limit. The important advancement in this theory is the conversion of the force-based transition from static to dynamic, into a velocity threshold definition (Hippmann, 2004). Calling v_t the tangential velocity modulus and v_s the velocity threshold, the friction force modulus F_t is defined in Eq. (12):

$$F_t = \begin{cases} \mu_d |F_n| & if\ v_t \geqslant v_s \\ \mu_d |F_n| \frac{v_t}{v_s}\left(2 - \frac{v_t}{v_s}\right) & if\ v_t < v_s \end{cases} \tag{12}$$

Here, μ_d is the Coulomb's dynamic friction coefficient. It is a regularized version of the Coulomb's law of dry friction: if the slip velocity falls below the threshold v_s, the friction force is faded out quadratically, as represented in Fig. 6.

As a first guess, transition velocity v_s (to be correctly tuned by experimental tests) was set equal to the Stribeck velocity that is the velocity at which the stick–slip effect occurs (in the Stribeck curve). It has been proven experimentally that a velocity threshold in the range between 10^{-4} and 10^{-6} m/s is a good compromise between the accuracy and computational effectiveness (Wojewoda et al., 2008). By definition, the acting direction of the friction force is always tangent to the surface and opposite of the relative velocity between the two sliding bodies.

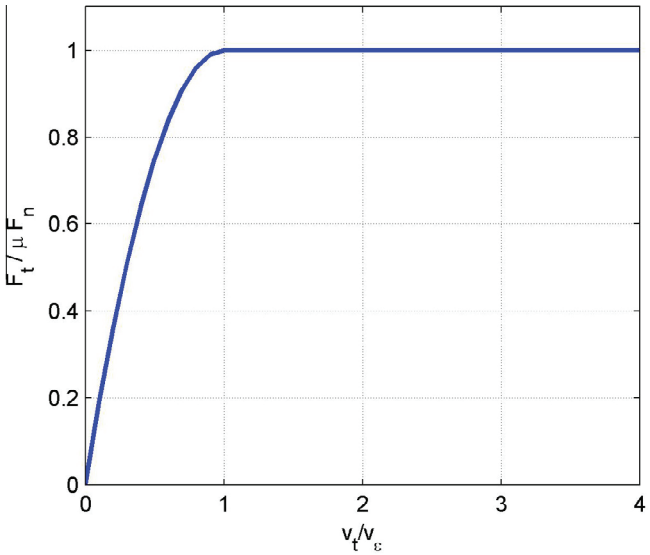

Fig. 6. Regularized version of Coulomb's friction law.

3. Simulation results

3.1. Tumbling target capturing and towing: in-orbit demonstration scaled scenario

In order to analyse the contact model and to clearly identify the fall-outs on system dynamics, the following simulations have run with a simplified cubical target without appendages or antennas. The following simulations refer to a scenario of an In-Orbit Demonstration (IOD) mission, envisaged to increase the technology readiness level (TRL) of net capturing systems. For this reason, the system has been dynamically scaled down with respect to a large satellite capture. In Table 1 the simulation parameters are reported.

In Fig. 7, the operations' sequence is represented in the chaser Local Vertical Local Horizontal Frame (LVLH, cf. Appendix A for a detailed explanation of the used reference systems), and the net shooting axis is along the orbital velocity direction (V-bar configuration); the tether linking the net to the chaser spacecraft is depicted in purple in the figure.

In Fig. 8, the maximum internal tensions on tether and net elements are represented, being these loads essentials for tethered-net's design and sizing. Besides the initial bouncing of the target towards the chaser, involving stresses overshooting and oscillations, the final forces stabilize and the exact thrusting action can be clearly visible in the tether transmitted force. The initial overshoot is due to the tether tensioning after the capture. By analysing contact forces and torques transmitted to the target by the net, represented in Fig. 9, it is possible to note that, coherently with the physics of the pulling, the transmitted action is mainly along V-bar (F_x) and equals the pulling force magnitude, while the other components are damped during towing. During the pulling phase, the flexible tether, as it is modelled, behaves as a spring-damper system: this leads to axial oscillations of the relative distance/velocity between the end-bodies, with a frequency directly related to the stiffness of the tether. Therefore, tension and contact forces present the same oscillations.

Table 1
IOD simulation parameters.

Net configuration	Planar	
Net size [m]	2 × 2	
Net mesh [m]	0.2	
Bullets #	4	
Bullet mass [kg]	0.07	
Bullet ejection velocity [m/s]	2	
Divergence angle [deg]	30	
Net mass [kg]	0.14	
Threads material	Technora	
Threads diameter [mm]	Perimeter and medians	Other threads
	2	0.5
Threads Young's modulus [GPa]	25	
Threads damping factor [–]	0.3	
Equivalent contact stiffness [N/m]	500	
Hysteresis damping factor [–]	0.5	
Friction factor [–]	0.1	
Target size [m]	0.5 × 0.5 × 0.5	
Target mass [kg]	83	
Target angular velocity [deg/s]	[1–5 1]	
Capture distance [m]	2.5	
Thrust [N]	15	
Burning time [s]	400	
Orbit	SS0 500 km	

Finally, it is possible to appreciate the contact model indirect effects, involving energy dissipation through slippage and friction: in Fig. 10 the target body angular momentum and angular velocities are reported. In simplified models, only taking into account a fixed non-slipping contact point between the tether and the target, the evolution of target angular velocity shows the so-called tail wagging effect, i.e. the periodic oscillation of the debris which appears as a stable limit cycle obtained after a short transient during towing, whose values are much bigger than the initial one (da Cruz Pacheco et al., 2013). After shutting down thrusters the target motion continues freely: this behaviour would be dangerous to carry out the operations both during pulling and during post-burn phases, risking entanglement with the tether, its breakage and possibly leading to chaser control authority loss. By contrast, in a complete model accounting for target slippage inside the net and friction effects, as in this case, the initial angular velocities and the further speeding-up contribution due to the initial shock torques (the so-called "whiplash effect") are clearly dissipated, proving the theorized effectiveness of the passive damping effect of tether–net capturing and demonstrating the importance of contact dynamics laws for the evolution of the overall dynamics. The frequency of target angular oscillations, perpendicular to tether axis, is also related to the tether stiffness while the amplitude depends on the target initial motion and net friction.

In Fig. 11 the final configuration with stabilized target, after 400 s pulling, is showed.

3.2. Tumbling target capturing: full scale scenario

A full scale capture scenario is represented in Fig. 12: the target is a low-detailed representation of the Envisat spacecraft in 800 km altitude sun-synchronous orbit (SSO), tumbling at 5 deg/s around its maximum inertia axis. The net is a 55 × 55 m planar net with 1 m square mesh, deployed by four bullets shot at 5 m/s; the total system mass (net, tether and bullets) is 8.3 kg. The synchronization of the net deployment with the target angular motion strongly affects the closing behaviour.

4. GNC and net system design

4.1. Towing and post-burn phases: de-orbiting simulation, feedback control and stabilization

The main design driver for a de-orbit system is the magnitude of the breaking manoeuvre to be performed.

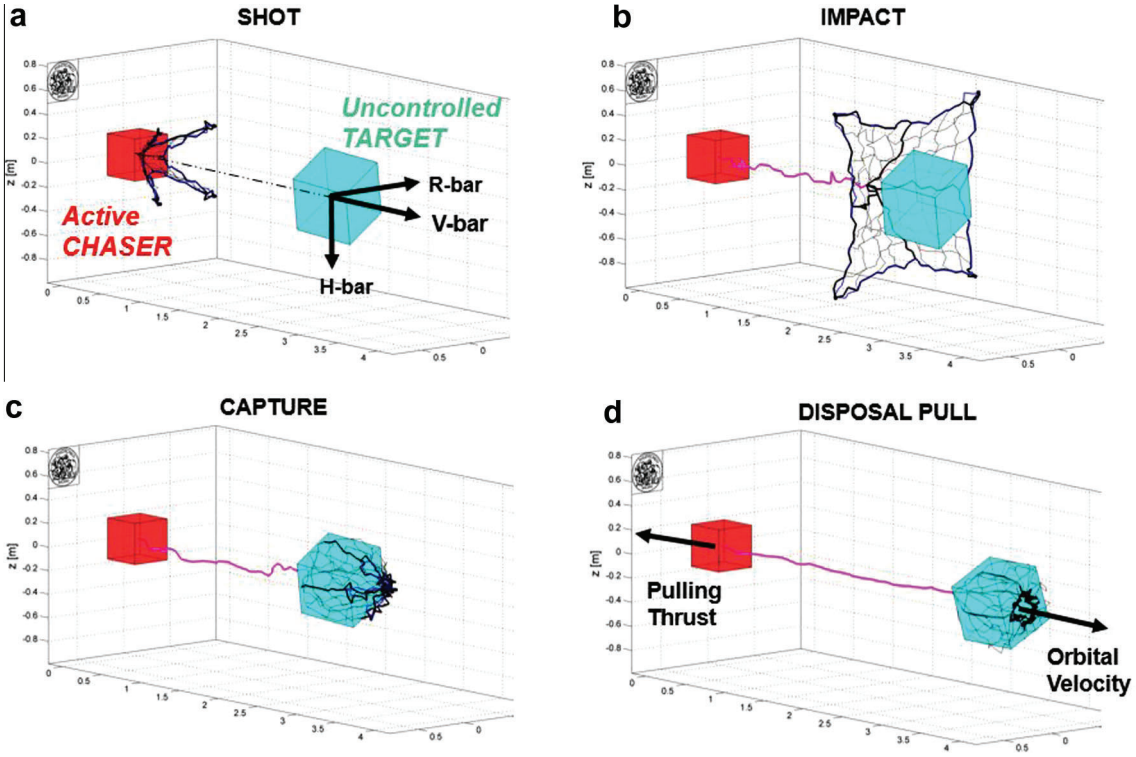

Fig. 7. Operations sequence represented in chaser LVLH frame.

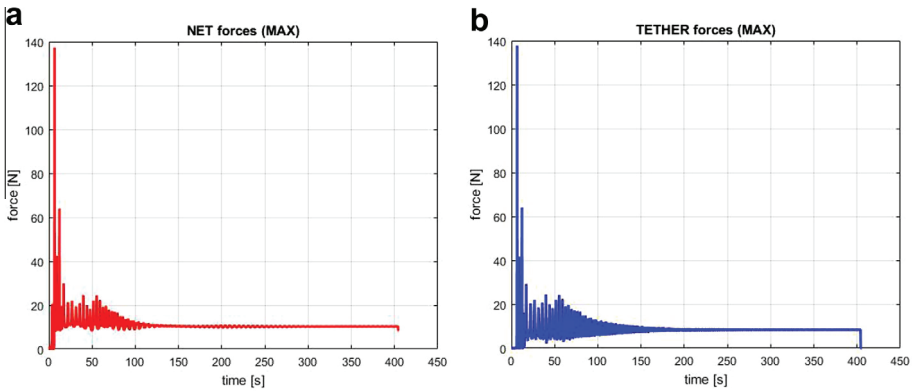

Fig. 8. Internal tensions on net (a) and tether (b) during capture and disposal phases.

A controlled de-orbiting, resulting in an immediate re-entry at a predefined position requires a high thrust propulsion system. In order to confine the impact area, it is necessary to have a sufficiently steep flight path angle, in the range of -1.5 to -2.5 deg, depending on initial orbit altitude, at the atmospheric window supposed to be at 120 km of altitude. A safe transportation process is possible when the thrust vector coincides with the direction of the tether and the tether is always tensioned. At the same time the chaser needs to keep thrust oriented with the anti-velocity direction to maximise the efficiency of the transfer and keep the system stable in the orbital plane with the chaser "behind" the target: it is demonstrated in the following how during thrusting periods the chaser shall be controlled to pull in the anti-velocity direction, the direction of the tether aligning by consequences. This allows to keep a stable rear position in orbital plane with respect to the target. Whenever the high thrust is shut down, the tether slackens and the residual tension makes the two objects accelerate towards each other, pulling them close: the risk of post-burn collisions is high especially with an elastic tether and shorter separation distances. This collision can dangerously increase uncertainty of the initial conditions of the space debris at the beginning of the atmospheric stage of the descent process. In any case, the control shall be recovered to avoid post-burn collisions whenever a

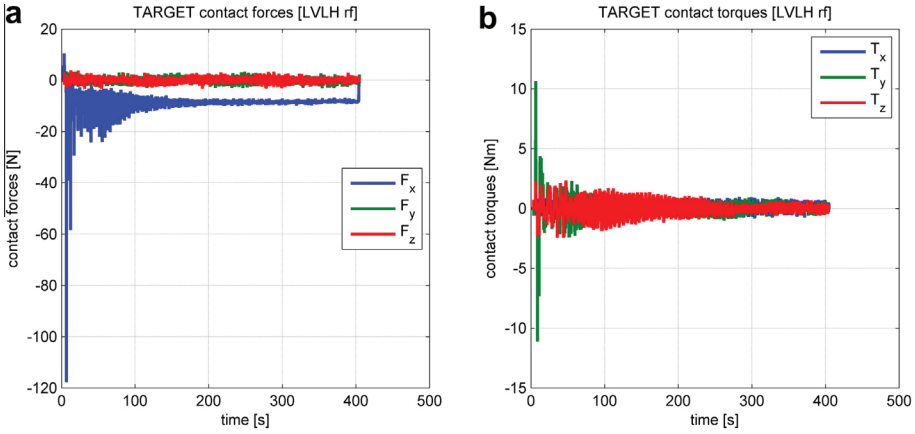

Fig. 9. Contact forces (a) and torques (b) acting on the target.

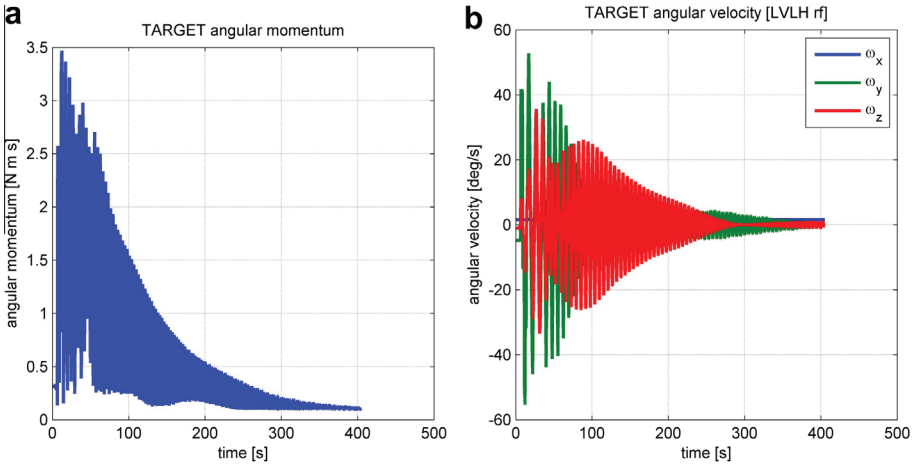

Fig. 10. Target angular momentum (a) and angular velocities in body frame (b).

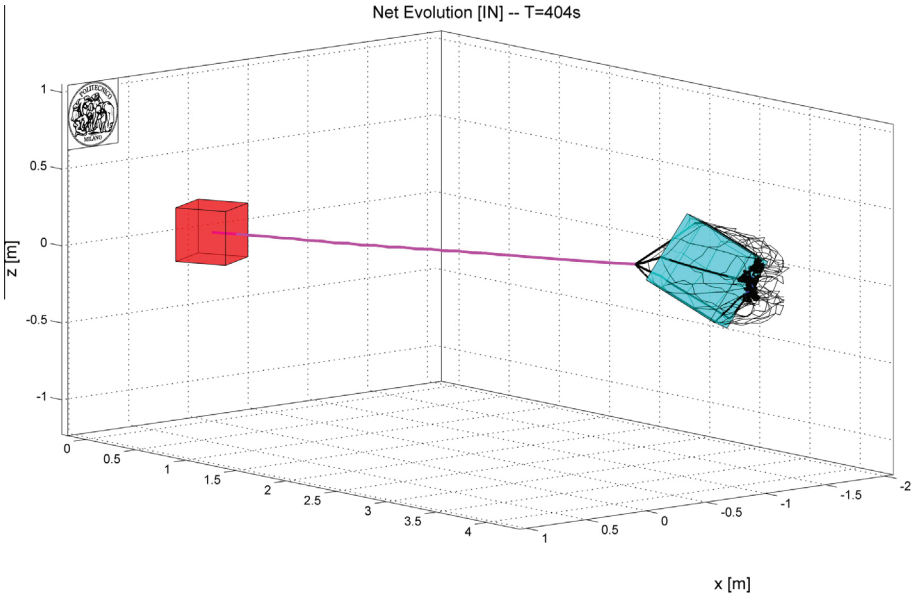

Fig. 11. Final time frame of simulated dynamics, after 400 s thrusting.

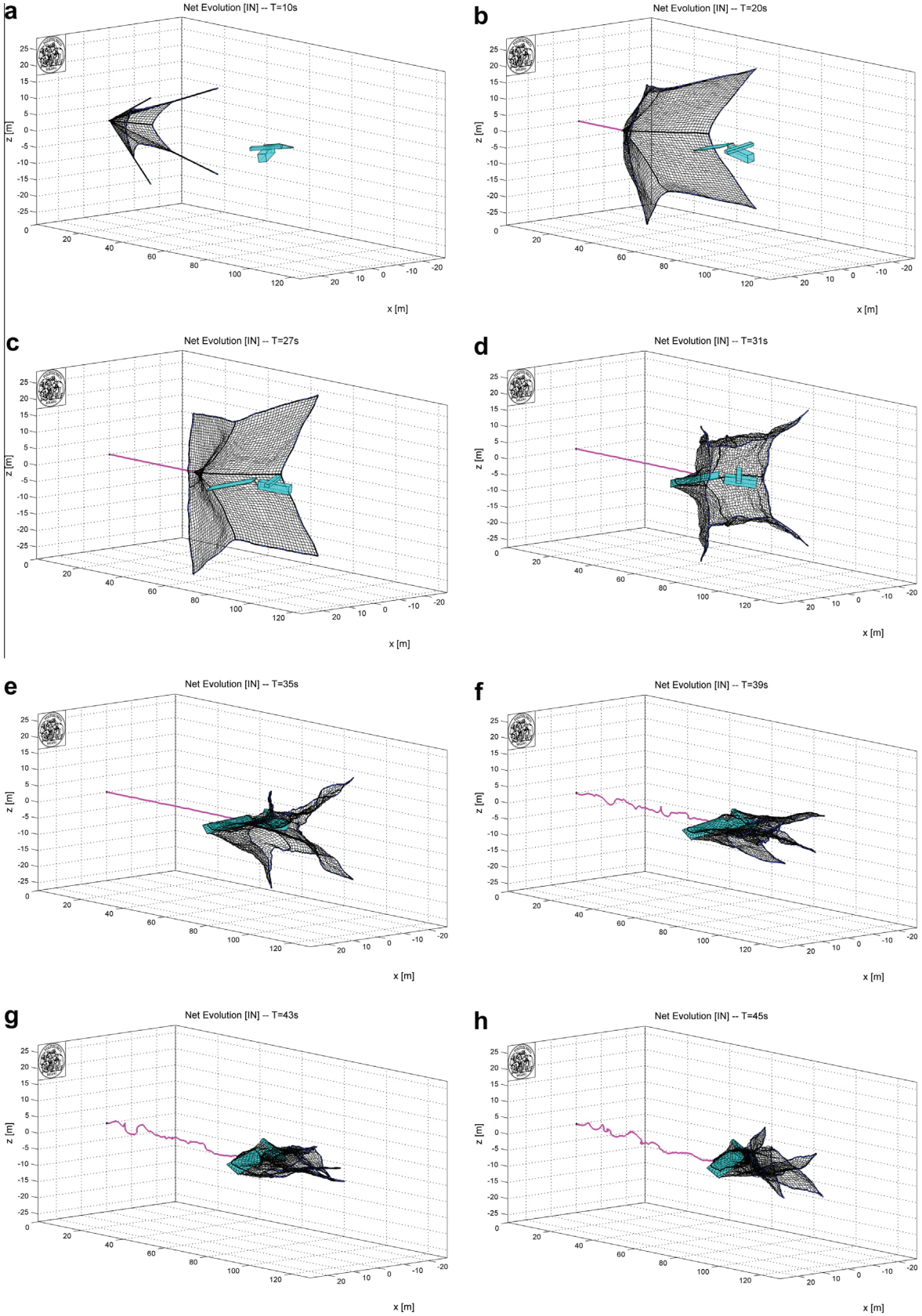

Fig. 12. Full scale capture sequence in LVLH frame.

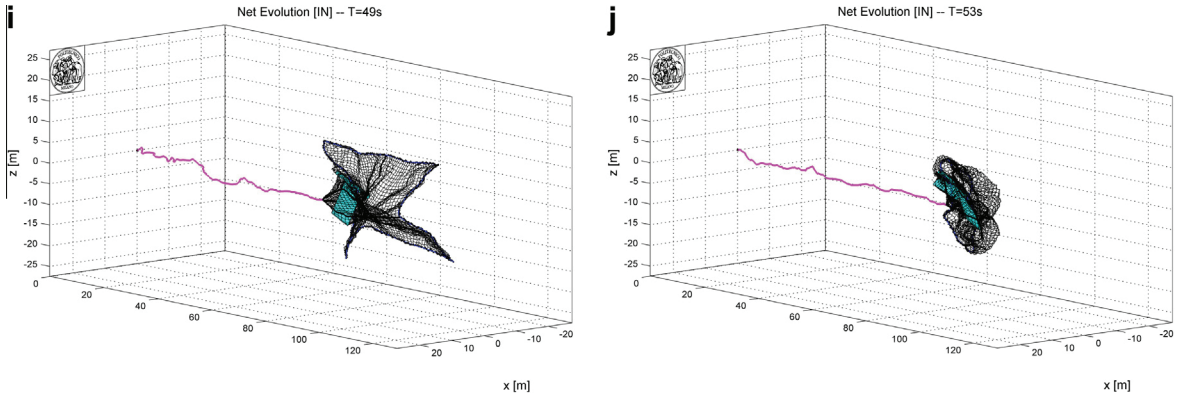

Fig 12. *(continued)*

Table 2
De-orbiting burn simulations parameters.

Chaser mass [kg]	1300	
Target mass [kg]	5000	
Initial orbit altitude [km]	600	
Thrust [N]	Main	RCS
	800	25
Burning time [s]	1300	
Tether Young's modulus [GPa]	32	
Tether damping [Ns/m]	16.62	
Tether length [m]	100	

multi-burn de-orbiting mission is carried out or whenever the chaser needs to be re-used to dispose of other objects during the same mission.

A closed loop control has been implemented to simulate the whole removal manoeuvre. The actual sensors dynamics has not been considered as part of this work: the loop is closed on the chaser absolute state and on the target relative position, supposed to be known with a good accuracy. The navigation is used to trigger different mission phases and switch control modes: the ignition and cut-off of thrusters and the switching between ACS modes is done in an

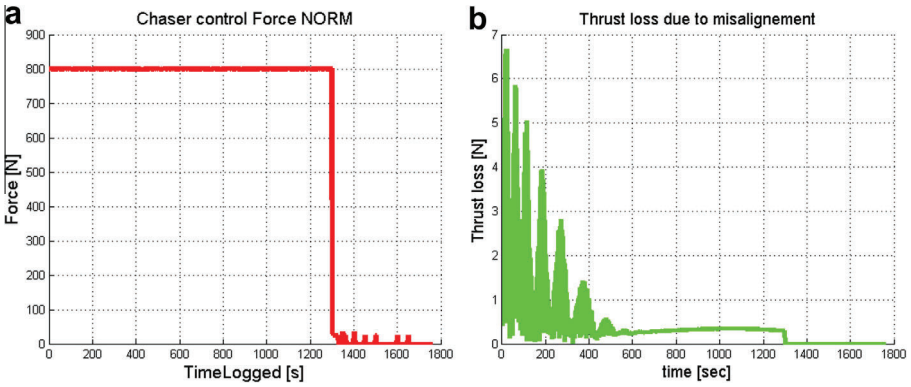

Fig. 13. De-orbiting simulation: chaser control force norm (a) and thrust losses (b).

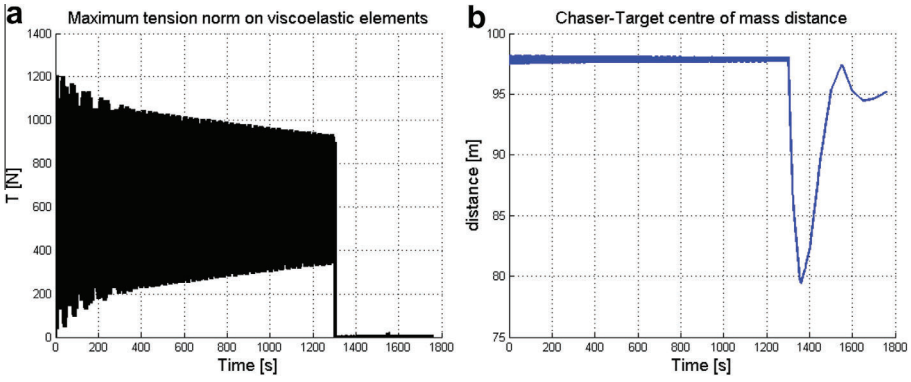

Fig. 14. De-orbiting simulation: tether tension (a) and chaser-target relative distance (b).

event driven fashion with feedback on states and tether tension or in a time driven way by defining the mission timeline a priori. The first mode has demonstrated to be more safe and effective, as expected. The guidance is closed loop during stabilization and relative manoeuvring and open loop during de-orbiting burns. Main engines are supposed to be controlled ON/OFF as well as reaction control system (RCS) engines. Relative position control is done using a proportional-derivative law and performed using RCS with pulse width modulation (PWM). Thrust vector control is performed through attitude control system (ACS). A proportional derivative attitude control has been implemented for the chaser through continued wheels' control. Two ACS modes have been set-up:

- relative to the target: to align the tether with the target direction avoiding entanglement;
- absolute: to align the thrust in the anti-velocity direction to maximise transfer efficiency.

The first is used during stabilization manoeuvres while the second is used during main burns. A steering law has also been implemented, exploiting the degree of freedom around tether axis, to correctly orientate chaser solar panels as perpendicular to sun direction as possible to maximise generated power. In Table 2, the controlled de-orbiting simulation parameters are listed.

The initial orbit is a circular dawn-dusk SSO. The starting epoch of the simulation is the spring equinox of 2022 to ease results interpretation. The chaser has installed onboard 2×400 N high thrust engines for de-orbiting burns and RCS thrusters giving 25 N on three axes. The tether's material is a high modulus – high tenacity (HMHT) synthetic fibre: a 3 millimetre diameter tether of Technora or Kevlar allows to withstand the loads, limit the mass and respect requirements on folding and environment. Tether length is supposed to be fixed during operations. Here, the pulling and post-burn control recovery are simulated. All the above mentioned perturbations have been accounted for. A single de-orbiting burn is here presented, however a multi-burn strategy can be conceived as long as the stability of the system is recovered after the burn: in this case several burns can be made at the apogee, gradually

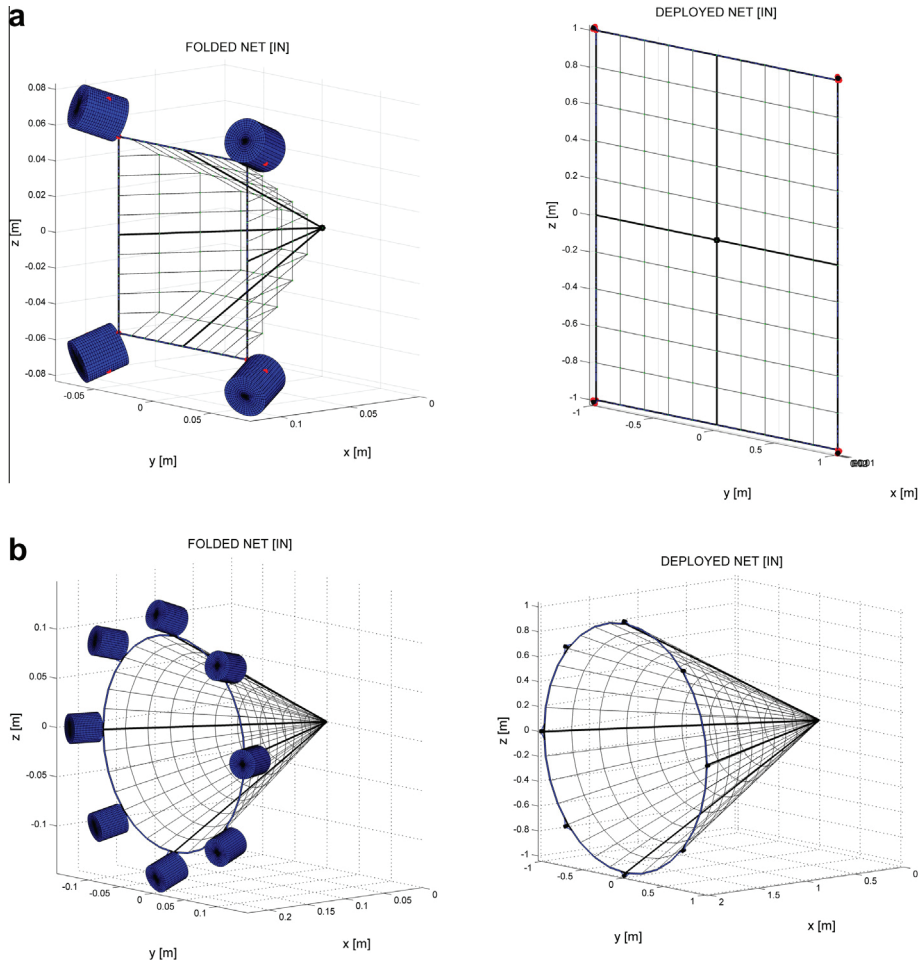

Fig. 15. Different net topologies in folded and deployed configurations: (a) planar with 4 bullets; (b) conical with 8 bullets.

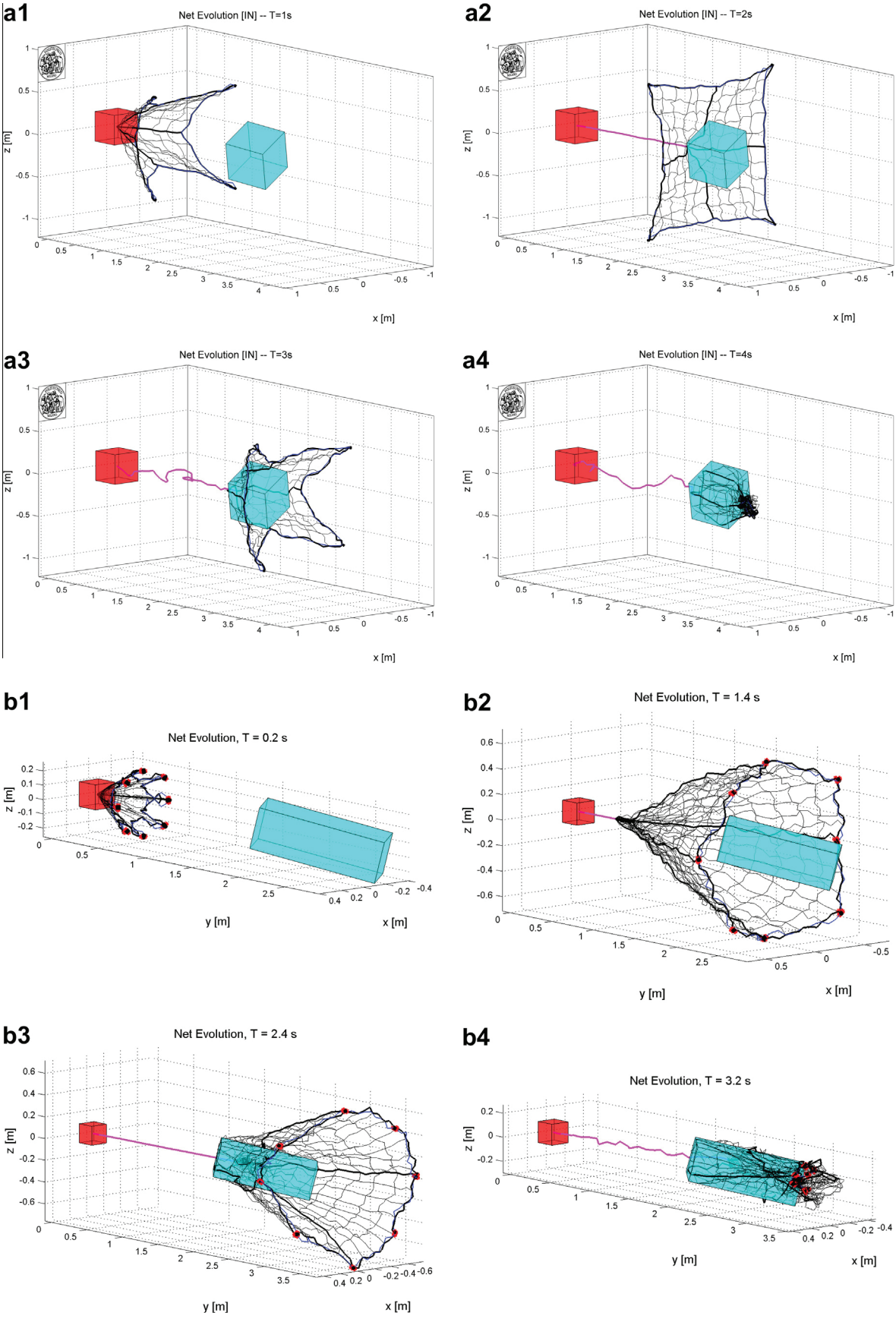

Fig. 16. Planar net capture sequence (a) versus conical net capture sequence (b).

reducing the perigee. However, this can only be done when the perigee is above the atmospheric interface.

With a burning time of 1300 s, the imparted Delta-V is 160 m/s and the flight path angle reached at 120 km of altitude is $-1.6°$. Expended fuel mass is 330 kg. Results are presented in Figs. 13 and 14. After 1300 s, the main thrust is shut down and only the RCS is working to stabilize the system: this second phase is characterised by the bouncing-back effect and the recovering of relative distance and stabilization of the stack.

Fig. 13a shows the control force applied to the chaser where after the main burn shut down, different pulses are present to recover control and stabilize the system in relative position. Fig. 13b describes the total thrust losses due to misalignment with the anti-velocity direction: the stretched tether being not exactly oriented with this direction. It is possible to remark how losses are always below 7 N and less than 1 N when equilibrium is reached. In Fig. 14a, the tension acting on the tether is represented, its level being far below the breaking strength of Aramidic fibres. The relative distance between the bodies is represented in Fig. 14b, to show the post-burn approach and the distance recovery through PWM control.

4.2. Net and closing mechanism design

The net design is the key feature of such a system: it must be appropriately light, strong and elastic. In particular, its elasticity strongly influences the overall dynamics behaviour. Candidate materials have been identified in HM–HT (high modulus–high tenacity) synthetic fibres, mainly aramid (as Kevlar or Technora) and HMPE (as Dyneema). In order to limit system masses and volumes, while meeting the requirements on strength and debris generation containment, nets are designed with reinforced perimeter and some internal threads (medians or diagonals) directly linked to the tether, to withstand pulling loads. The secondary threads have a decreased diameter and have function of both containment and motion damping through friction, as explained in the following paragraphs.

A closing mechanism may be mandatory to ensure a successful capture and a safe de-orbit pulling. To ensure the closure of the net a thread ring is introduced at the net mouth and it is wound by winches inside the bullets: these winches are supposed to be a couple of counter-rotating reels to avoid torque effects on the bullets. This event-driven control applied to winches has demonstrated, through simulations, to be more reliable than a time-driven control: however, a delay between impact detection and closing command, dependent on the target-net geometrical features, is introduced to guarantee the net correct closure. During the closure, the closing links' winding is simulated reducing the nominal length of these links, generating the stress responsible for the closure on the nodes where they are attached. The closing thread are modelled as any other threads except for their variable length: the length can be externally controlled at any time to simulate winding and unwinding. A change in element length leads to a change in stiffness, damping and mass: properties changes of all nodes/elements belonging to the same threads are equally distributed. Each rolled/unrolled thread mass is added/removed on the which (supposed to be contained inside the bullets) responsible for that thread. Slippage of threads on the knots due to interlacing has not been considered so far. A linear control law has been implemented for the closing threads, controlling their length in an event-driven way (the closing law is activated whenever the impact between tether and net is detected).

The net shape can be either planar or three-dimensional (i.e. conical or pyramidal). As examples, a planar net with reinforcements is represented in Fig. 15a, in both folded and deployed configuration (note the bullet size with respect to the two configurations), while a conical net with 8 bullets, in both configurations, is represented in Fig. 15b. A quadrangular mesh has been selected, being the optimum compromise between total mass and out-of-plane stiffness. Square mesh has also the ability to withstand large shearing deformations without requiring creases in the material, which is an important characteristic for folding and packaging.

Fig. 16 depicts the capture and closure sequences of both planar and conical nets presented above. The reference system is, as previous simulation output, the Local Vertical Local Horizontal (LVLH, cf. Appendix A), centred on the chaser.

By analysing simulations results, the following considerations are possible:

- Conical and planar nets have different capturing behaviours: while the planar net mainly relies on impact and wrapping, three-dimensional nets, such as the conical one, envelope the target not necessarily impacting with it. Therefore, it is possible to conclude that the second type of capturing is safer and more reliable but on the other hand it requires bigger nets (the target needs to be totally enveloped before impact) and a closing mechanism is mandatory, with an obvious increase in masses and volumes.
- By contrast with planar nets, conical nets can be deployed by a number of bullets greater than 4, which may be safer and more reliable in case of bullets' shooting failures.
- The closing mechanism, as it is simulated, has proven to be effective. However, experimental tests are needed to tune the design, characterise performance and verify functionalities.

5. Conclusions

In this paper, a complete and physically-based mathematical model of a tethered-net device for active space debris removal is presented. The main goal of this simulator is

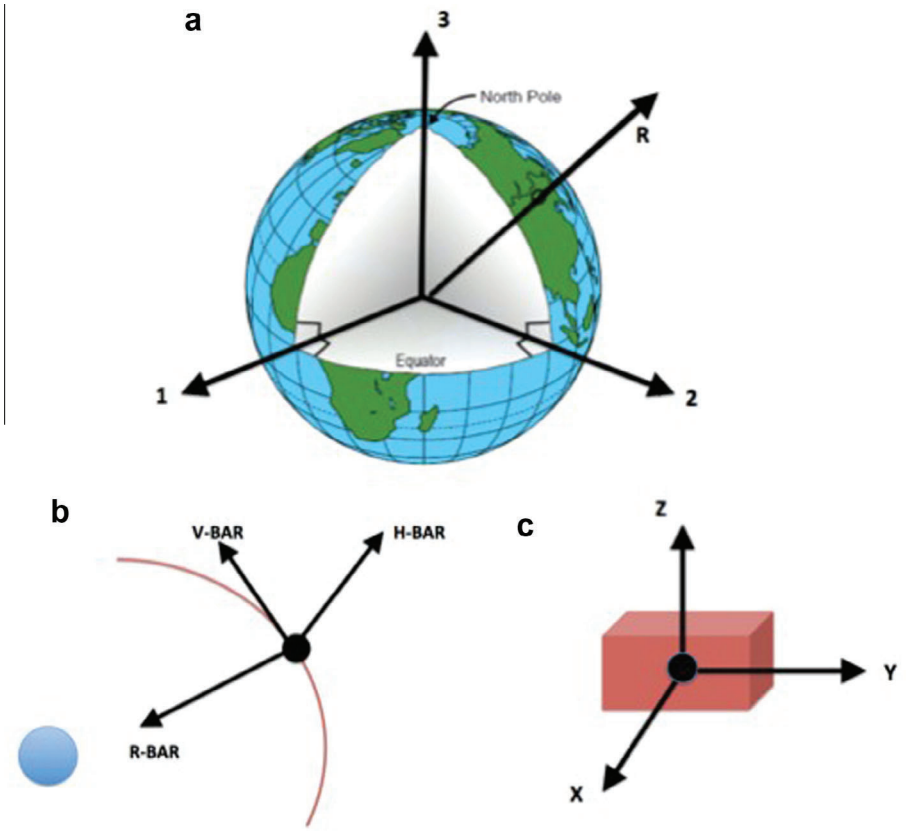

Fig. A-1. Reference frames: (a) ECI, (b) LVLH, (c) BODY.

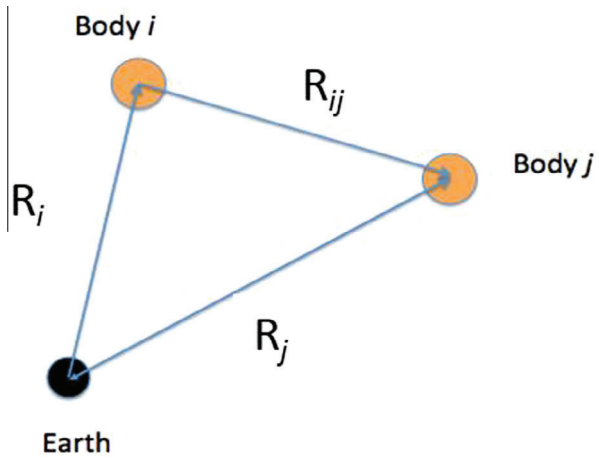

Fig. A-2. Relative position convention.

to support the design of such flexible ADR system: it revealed to be a useful tool to describe the overall dynamic behaviour and the unforeseen dynamics arising from the interaction between two isolated bodies, becoming a single multibody system to deorbit. In particular, most of the attention was put on the interface between the net and the free-tumbling object during the disposal pull.

Results have shown the great role played by the contact modelling, proving energy dissipation and therefore reducing both the axial bouncing dynamics of the target during the pull and the target angular momentum content. These translate into a major benefit for the net-device concept, providing a passive damping aid. This effect is extremely important from a control point of view, helping the stabilization of the stack: it is demonstrated how the passive angular motion damping allows the chaser to keep the control authority during the most delicate phases of the mission.

The capture system design has been addressed and the design drivers have been formulated as an outcome of the dynamics analysis results: different net shapes have been analysed and their difference have been presented in the paper. A net configuration design, allowing reducing the system mass, have also been proposed. The net has been provided with a closing mechanism: an interlaced thread on the net perimeter (e.g. its mouth) is wounded by reels inside the bullets to close the net mouth around the target. The closing mechanism is activated at impact occurrence with a delay depending on the net velocity and target features and it guarantees a safe and firm grasping during towing.

Recently, a microgravity experimental campaign has been executed to validate both the flexible dynamics and the contact dynamics models implemented in the presented simulator. The experiment was successfully conducted on

June 9th 2015 in the Novespace 116th parabolic flight campaign (62nd ESA Parabolic Flight campaign) on-board an Airbus A310 ZERO-G aircraft. The parabolic flight experiment also allowed raising the technology readiness level (TRL) of space throw-net techniques to TRL 5 (i.e. representative prototype tested in a relevant environment). Data are currently being analysed and the full model validation and update are expected within the next few months.

By providing a passive stabilization of the stack during disposal, reducing the tail-wagging effect and allowing multi-burn disposal strategies, tethered-net devices appear to be promising, presenting the most benefits with respect to other proposed ADR strategies, as demonstrated by an advanced simulation environment.

Acknowledgements

The authors acknowledge the European Space Agency TEC-ECN and TEC-MMA divisions for supporting studies related to the topic here discussed.

Appendix A

Dynamics models and equations of motion

Within the net deployment dynamics, the following references frames are defined:

- Earth Centred Inertial (ECI), centred in the Earth:
  - o **1-axis** permanently fixed towards the vernal equinox;
  - o **2-axis** in the Earth equatorial plane, right-hand side orthogonal to 1–3;
  - o **3-axis** lies at a 90° angle to the equatorial plane and extends through the North Pole.

- Local Vertical-Local Horizontal reference frame (LVLH), centred in the system centre of gravity:
  - o **R-bar** (X) axis towards the main attractor;
  - o **V-bar** (Y) transverse axis (along the target velocity direction if circular orbit), orthogonal to H-R.
  - o **H-bar** (Z) axis opposite to the angular momentum of the orbit;

- Body reference frame, (BODY) centred in the body centre of mass, the axis definition, X-axis, Y-axis, Z-axis, depending on the body inertia matrix definition I.

These reference frames are represented in Fig. A-1.

Vectors, quaternions and matrix are written here in bold characters. Each body centre of mass coordinate system is defined with respect to the ECI frame called world: any physical variable expressed with respect to this frame is be referred as absolute and indicated with a capital letter; for example $\boldsymbol{R_i}$ and $\boldsymbol{V_i}$ are the position and velocity vectors of body i in ECI frame. On the other hand, quantities referred to BODY coordinate system are indicated with a lowercase letter: for example $\boldsymbol{r_i}$ is the position an of point i in BODY frame. Double indexes indicate relative distance between two points: for example, $\boldsymbol{R_{ij}} = \boldsymbol{R_j} - \boldsymbol{R_i}$, is the relative position vector expressed in ECI frame between body i and j, pointing from i com towards j com as represented in Fig. A-2.

Rigid body kinematics is described by rotation quaternions. A quaternion is defined as

$$\boldsymbol{q} = \begin{Bmatrix} lv_1 \\ v_2 \\ v_3 \\ s \end{Bmatrix} = \begin{Bmatrix} le_1 \sin\frac{\theta}{2} \\ e_2 \sin\frac{\theta}{2} \\ e_3 \sin\frac{\theta}{2} \\ \cos\frac{\theta}{2} \end{Bmatrix} \tag{13}$$

where the last element is defined as the scalar part or real part, representing the cosine term of the rotation angle, and the first 3 elements represent the vector part (vector v) or imaginary part. A vector transformation from frame A to frame B, by means of the rotation quaternion, is performed with Eq. (14):

$$\begin{bmatrix} 0 \\ \boldsymbol{v_B} \end{bmatrix} = \boldsymbol{q_{BA}} \begin{bmatrix} 0 \\ \boldsymbol{v_A} \end{bmatrix} \boldsymbol{q^*_{BA}} \tag{14}$$

where

- $\boldsymbol{v_A}$ is a vector in the frame A;
- $\boldsymbol{q_{BA}}$ is the quaternion from frame A to frame B;
- $\boldsymbol{q^*_{BA}}$ is the conjugate of $\boldsymbol{q_{BA}}$;
- $\boldsymbol{v_B}$ is the vector in the frame B.

As a quaternion represents a rotation from one frame to another frame, the quaternion multiplication can multiply this kind of frame transformations, as expressed by the following:

$$\boldsymbol{q_{CA}} = \boldsymbol{q_{CB}} \cdot \boldsymbol{q_{BA}} \tag{15}$$

where

- $\boldsymbol{q_{CA}} = \boldsymbol{q_{A\to C}}$ is the quaternion from frame A to frame C;
- $\boldsymbol{q_{CB}} = \boldsymbol{q_{B\to C}}$ is the quaternion from frame B to frame C;
- $\boldsymbol{q_{BA}} = \boldsymbol{q_{A\to B}}$ is the quaternion from frame A to frame B.

The adopted convention is:

- $\boldsymbol{q_{absolute}}$ the quaternion from ECI frame to BODY frame;
- $\boldsymbol{q_{oribital}}$ the quaternion from ECI frame to LVLH frame;
- $\mathbf{q_{attitude}}$ the quaternion from LVLH to BODY.

Therefore, it is also:

$$\boldsymbol{q_{absolute}} = \boldsymbol{q_{attitude}} \cdot \boldsymbol{q_{orbital}} \tag{16}$$

Newton's equations of dynamics are described in ECI frame, in order not to model fictitious forces. Euler's equations are derived in body frame, instead. The gravitational forces and torques are applied to each body independently, depending on its absolute position and attitude. Torques are not applied to point masses for obvious reasons: rotational dynamics is not described for point masses.

The gravitational force, acting on body (or element) i, is defined as:

$$\boldsymbol{F_{Gi}} = -\frac{\mu m_i}{|\boldsymbol{R_i}|^3}\boldsymbol{R_i} \tag{17}$$

where
- μ the gravitational constant;
- m_i the element mass i;
- $\boldsymbol{R_i}$ the vector position of element i in ECI frame.

The gradient gravity torque is given for mass i by Eq. (18):

$$\boldsymbol{M_{Gi}} = -\frac{3\mu}{|\boldsymbol{R_i}|^3}\boldsymbol{c_i} \times \boldsymbol{I_i}\boldsymbol{c_i} \tag{18}$$

where $\boldsymbol{I_i}$ is the inertia matrix of body I and $\boldsymbol{c_i}$ is the vector of the direction cosines of the radial position of the body i com expressed in body axis as of Eq. (19).

$$\boldsymbol{c_i} = \frac{\boldsymbol{r_i}}{|\boldsymbol{r_i}|} \tag{19}$$

Chaser, target and bullets

Target and chaser are parallelepiped bodies defined by:

- mass M and inertia $\boldsymbol{I}$;
- three linear dimensions in BODY frame [a, b, c];
- tether connection point expressed in BODY frame;
- initial position $\boldsymbol{R_o}$, velocity $\boldsymbol{V_o}$, angular velocity $\boldsymbol{\omega_o}$ and orientation $\boldsymbol{q_o}$ wrt ECI frame.

The target is non cooperative and uncontrolled while the chaser can be controlled. In the following equations, the subscript T refers to the target, while C to the chaser.

The non-linear dynamics of the target is given in Eqs. (20) and (21):

$$M_T\frac{d^2\boldsymbol{R_T}}{dt^2} = \boldsymbol{F_{GT}} + \boldsymbol{F}_C + \boldsymbol{F}_{ext} \tag{20}$$

$$\boldsymbol{I_T}\dot{\boldsymbol{\omega}}_{\boldsymbol{T}} + \boldsymbol{\omega_T} \times \boldsymbol{I_T}\boldsymbol{\omega_T} = \boldsymbol{M_{GT}} + \boldsymbol{M_C} + \boldsymbol{M_{ext}} \tag{21}$$

where
- M_T, $\boldsymbol{R_T}$, $\boldsymbol{I_T}$, $\boldsymbol{\omega_T}$ are respectively target mass, centre of gravity position in ECI frame, inertia matrix and angular velocity in BODY frame;
- $\boldsymbol{F_{GT}}$ and $\boldsymbol{M_{GT}}$ is the gravitational force acting on target as expressed in Eqs. (17) and (18);
- $\boldsymbol{F_C}$ and $\boldsymbol{M_C}$ are the contact force and torque acting on target, as a result of the sum of contribution of each element of the target mesh;
- $\boldsymbol{F_{ext}}$ and $\boldsymbol{M_{ext}}$ are external forces and torques given by external inputs (for example perturbations).

The equations of motion for the chaser are given by:

$$M_C\frac{d^2\boldsymbol{R_C}}{dt^2} = \boldsymbol{F_{GC}} - \boldsymbol{T}_{12} + \boldsymbol{F}_{ext} \tag{22}$$

$$\boldsymbol{I_C}\dot{\boldsymbol{\omega}}_{\boldsymbol{C}} + \boldsymbol{\omega_C} \times \boldsymbol{I_C}\boldsymbol{\omega_C} = \boldsymbol{M_{GC}} + \boldsymbol{M}_{T12} + \boldsymbol{M_{ext}} \tag{23}$$

where, a part now obvious terms, $\boldsymbol{T_{12}}$ and $\boldsymbol{M_{T12}}$ are the reaction force and torque exercised by the tether on the chaser, as defined in Eqs. (1) and (25).

Bullets are cylindrical rigid bodies defined by their mass, inertia and net connection point. Their motion is described by six scalar equations, as (22) and (23), not repeated here, where reactions due to elements in tension are taken into account for all the connected threads and connection points, if multiple connections are applicable. Bullets have time varying mass depending on the length variation and consequent mass variation of closing threads.

Tether and net

Cables and ropes, such as the tether and net, are modelled with the lumped-parameter method, also called beads model. Tether/net ropes are defined by:

- rope length L_T;
- rope diameter D_T;
- Young modulus E_T;
- damping coefficient d_T;
- material density ρ_T;
- n number of discretization elements.

The length of each rope is supposed to have a fixed length during forward dynamics propagation, except for closing threads whose properties are time varying (mass, stiffness and damping depending on the actual user-controlled length).

The tether is discretized with n_T point masses, nominal length between two masses $l = L_T/n_T$ and equal mass $m_i = m_T/n_T$, connected by spring-dampers, Eq. (1), that can only exchange axial forces under tension (no forces exchanged under compression).

The equations of motions for masses $i = [2 - n]$ are given by:

$$m_i\frac{d^2\boldsymbol{R_i}}{dt^2} = \boldsymbol{F_{Gi}} + \sum_{j=-1,1}\boldsymbol{T}_{i,i+j} + F_{C_i} + F_{exti} \tag{24}$$

and for the first mass it is:

$$m_1\frac{d^2\boldsymbol{R}_1}{dt^2} = \boldsymbol{F_{G1}} + \boldsymbol{T}_{12} + F_{C_1} + F_{ext1} \tag{25}$$

where, a part from terms already defined above, it is:
- $\boldsymbol{T}_{Ti,i+j}$ the tension between the mass i and $i+j$, depending on their relative position and velocities as detailed in Eqs. (1)–(3);
- $\boldsymbol{F_{C_i}}$ is the contact force acting on each bead of the tether.

In a general net configuration, the Newton's equation for a mass m_i ($i = 1$ to total number of net knots) is given by:

$$m_i \frac{d^2 \boldsymbol{R_i}}{dt^2} = \boldsymbol{F_{Gi}} + \sum_{j=l} \boldsymbol{T}_{i,i+j} + \boldsymbol{F}_{ext} \tag{26}$$

where $j = l$ is the index number of all masses connected through an element rope to that knot i.

References

Andrenucci M., Pergola P., Ruggiero A., 2011. Active removal of space debris – expanding foam application for active debris removal, Ariadna study report 10-4611, European Space Agency, Advanced Concepts Team. Available on line at <www.esa.int/act>.

Aslanov, V.S., Ledkov, A.S., 2012. Dynamics of tethered satellite systems. Woodhead, Oxford, ISBN 978-0-85709-156-7.

Aslanov, V., Yudintsev, Y., 2013. Dynamics of large space debris removal using tethered space tug. Acta Astronaut. 91, 149–156.

Aslanov, V., Yudintsev, Y., 2013. Dynamics of large debris connected to space tug by a tether Samara state aerospace university, 443086, Russia. J. Guidance, Control, Dyn. http://dx.doi.org/10.2514/1.60976.

Astrium, Robotic Geostationary Orbit Restorer (ROGER) Phase A final report, 26 June 2003. ROGSIBRE-FP, Issue 1.

Bastida, B., Krag, H., 2011. Analyzing the criteria for a stable environment. In: Proc. 2011 AAS/AIAA Astrodynamics Specialist Conference, Girdwood, Alaska.

Biesbroek, R., et al., 2013. The e.Deorbit study CDF study: a design study for the safe removal of a large space debris. 6th IAASS Conference, Montréal, Canada, 22/05/2013.

Bombardelli, C., Pelaez, J., May 2011. Ion beam shepherd for contactless space debris removal. J. Guidance, Control, Dyn. 34 (3), 916–920.

Botta, E.M., Sharf, I., Misra, A.K., January 11–15, 2015. On the modelling and simulation of tether-nets for space debris capture. In: Proc. of 25th AAS/AIAA Space Flight Mechanics Meeting, Williamsburg, VA, USA.

da Cruz Pacheco, G.F., Carpentier, B., Petit, N., April 22–25, 2013. De-orbiting of space debris by means of a towing cable and a single thruster spaceship: whiplash and tail wagging effects. In: Proc. 6th European Conference on Space Debris, Darmstadt, Germany.

Gilardi, G., Sharf, I., 2002. Literature survey of contact dynamics modelling. Mech. Mach. Theory 37 (10), 1213–1239. http://dx.doi.org/10.1016/S0094-114X(02)00045-9.

Gonzalez-Vallajo, J., Fehse, W., Tobias, A., 1992. A multipurpose model of Hermes-Columbus docking mechanism. In: 26th Aero Mechanisms Symposium, pp. 297–313, Greenbelt.

Hardt, M., Mas, C., Ayuso, A., Cocho, D., Mollinedo, L, Gracia, O., Urmston, P., 2011. Validation of space vehicle docking with the international berthing & docking mechanism and a kuka robot. In: 14th European Space Mechanisms and Tribology Symposium, Konstanz.

Hippmann, G., 2004. An algorithm for compliant contact between complexly shaped surfaces in multibody dynamics. Multibody Syst. Dyn. 12 (4), 345–362.

Hobbs, S., 2010. Debris removal from low earth orbit Dr LEO. Cranfield University, College of Aeronautics Report, 1001. ISBN 978-1-907413-04-9.

Huang, P., Zehong, H., Zhongjie, M., 2015a. Coupling dynamics modelling and optimal coordinated control of tethered space robot. Aerosp. Sci. Technol. 41 (2015), 36–46.

Huang, P., Wang, D., Meng, Z., Zhang, F., 2015b. Adaptive postcapture backstepping control for tumbling tethered space robot-target combination. AIAA J. Guidance Control Dyn. http://dx.doi.org/10.2514/1.G001309.

Huang, P., Zhang, F., Ma, J., Meng, Z., Liu, Z., 2015c. Dynamics and configuration control of the maneuvering-net space robot system. Adv. Space Res. 55 (2015), 1004–1014.

Hunt, K., Crossley, H., 1975. Coefficient of restitution interpreted as damping in vibroimpact. Trans. ASME, J. Appl. Mech. 42 (2), 440–445. http://dx.doi.org/10.1115/1.3423596, 6 pages.

Jasper, L., Schaub, H., April 2013. Input shaped large thrust maneuver with a tethered debris object. In: 6th European Conference on Space Debris, ESOC, Darmstadt, Germany. <http://Hanspeterschaub.info/papers/jasper2013.pdf>.

Jasper, L., Schaub, H., Seubert, C., Valery, T., Yutkin, E., 2012. Tethered tug for large low earth orbit debris removal. In: Proc. of the AAS/AIAA Astrodynamics Specialists Conference (AAS12-252), Charleston, SC.

Johnson, K.L., 1987. Contact Mechanics. Cambridge University Press, London, ISBN 0-521-34796-3.

Liou, J.C., Johnson, N.L., 2007. A sensitivity study of the effectiveness of active debris removal in LEO. In: Proc. 58th IAC 'International Astronautical Congress' (IAC-07-A6.3.05), Hyderabad, India.

Nishida, S., Yoshikawa, T., 2003. Space debris capture by a compliance controlled robot, National Aerospace Laboratory of Japan. In: Proc. of the 2003 IEEE/ASME.

Nishida, S., Yoshikawa, T., 2007. Capture and motion braking of space debris by a space robot. In: Proc. of International Conference on Control, Automation and Systems, Seoul, 17–20 Oct. 2007. http://dx.doi.org/10.1109/iccas.2007.4406990.

Rabinowicz, E., 1956. Stick and slip. Sci. Am.

Rank, P., Mühlbauer, Q., Naumann, W., Landzettel, K., 2011. The DEOS automation and robotics payload, 11th Symposium on Advanced Space Technologies in Robotic and Automation, ESA/ESTEC, Noordwijk, The Netherlands, 12–14 April 2011.

Reed, J., Busquets, J., White, C., 2012. Development of a Grappling System for Capturing Heavy Space Debris. IAC-12- A6.5.17. 63rd International Astronautical Congress.

Seweryn, K., Banaszkiewicz, M., Maediger, B., Rybus, T., Sommer, J., 12–14 April 2011. Dynamics of space robotic arm during interactions with non-cooperative objects. 11th Symposium on Advanced Space Technologies in Robotic and Automation, ESA/ESTEC, ESA/ESTEC, Noordwijk, The Netherlands.

Wang, D., Huang, P., Meng, Z., 2015. Coordinated stabilization of tumbling targets using tethered space manipulators. IEEE Trans. Aerosp. Electron. Syst. 51 (3). http://dx.doi.org/10.1109/TAES.2015.140530.

Wojewoda, J., Stefański, A., Wiercigroch, M., Kapitaniak, T., 2008. Hysteretic effects of dry friction: modelling and experimental studies. Philos. Trans. Roy. Soc. A: Math., Phys. Eng. Sci. 366 (1866). http://dx.doi.org/10.1098/rsta.2007.2125.

Wormnes, K., Le Letty, R., Summerer, L., Schonenborg, R., Dubois-Matra, O., Luraschi, E., Cropp, A., Krag, H., Delaval, J., 2013. ESA technologies for space debris remediation. In: Proc. 6th European Conference on Space Debris, Darmstadt, Germany.

Wormnes, K., de Jong, J.H., Krag, H., Visentin, G., 2013. Throw-nets and tethers for robust space debris capture. In: 64th International Astronautical Congress, IAC-13, A6.5, 2x16445, Beijing, China.

Zachmann, G., 2000. Virtual reality in assembly simulation – collision detection, simulation algorithms and interaction techniques. PhD thesis, Department of Computer Science, Darmstadt University of Technology, 2000. Computer Graphik Edition, 3, ISBN: 3-8167-5628-X, ISBN: 978-3-8167-5628-6.